

Variational Probabilistic Fusion Network for RGB-T Semantic Segmentation

Baihong Lin*, Zengrong Lin*, Yulan Guo, Yulan Zhang, Jianxiao Zou, Shicai Fan

Abstract—RGB-T semantic segmentation has been widely adopted to handle hard scenes with poor lighting conditions by fusing different modality features of RGB and thermal images. Existing methods try to find an optimal fusion feature for segmentation, resulting in sensitivity to modality noise, class-imbalance, and modality bias. To overcome the problems, this paper proposes a novel Variational Probabilistic Fusion Network (VPFNet), which regards fusion features as random variables and obtains robust segmentation by averaging segmentation results under multiple samples of fusion features. The random samples generation of fusion features in VPFNet is realized by a novel Variational Feature Fusion Module (VFFM) designed based on variation attention. To further avoid class-imbalance and modality bias, we employ the weighted cross-entropy loss and introduce prior information of illumination and category to control the proposed VFFM. Experimental results on MFNet and PST900 datasets demonstrate that the proposed VPFNet can achieve state-of-the-art segmentation performance.

Index Terms—RGB-T semantic segmentation, probabilistic fusion, modality noise, class-imbalance, modality bias

I. INTRODUCTION

RGB-based semantic segmentation aims at categorizing each pixel in a RGB image into a specific class, which has been applied in many domains, including robot vision, autonomous driving, and path planning [1]–[4]. Unfortunately, a RGB image is sensitive to illumination, thus, recent studies propose RGB-T semantic segmentation, i.e., semantic segmentation based on the fusion of paired RGB and thermal images, to deal with poor illumination caused by low-light, rainy, and foggy conditions [5]–[7].

So far, deep learning methods have been widely adopted for RGB-T semantic segmentation, since they usually work excellently in many existing datasets. To achieve good segmentation performance, it is important that how to effectively fuse the deep complementary features from both RGB and thermal images. Early studies directly fuse deep features of RGB and thermal images by simply adopting element-wised addition or

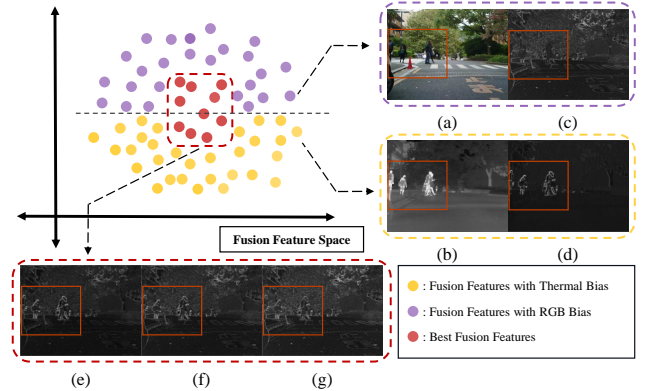


Fig. 1. Illustration of the assumption that the optimal features for semantic segmentation are a series of fusion features within a certain range. Circles represent fusion features. (a)-(d) Original RGB image, thermal image and their features, respectively. (e)-(g) A series of different fusion features which can achieve equally good semantic segmentation performance.

concatenation. But these designs ignore the modality differences between RGB and thermal images, leading to inadequate cross-modality complementary information exploitation [7]. To solve the above problem, recent studies provide different fusion designs: Some researchers introduce attention mechanisms for features of RGB and thermal images before fusion to reduce the modality differences [7]–[9]; others leverage prior information, such as object boundaries and contours, to guide the feature generation and fusion processes, thereby preserving relevant information from both modalities [6], [10], [11]. These fusion designs have been demonstrated to enhance the performance of RGB-T semantic segmentation.

However, existing methods are limited by the implicit assumption that the optimal fusion feature of RGB and thermal images is unique for the following reason: First, the unique fusion assumption will weaken generalization ability, since the fusion feature is usually vulnerable to class-imbalance [12], modality bias [13], and modality noise [14]. Second, this assumption limits feature representation ability, thus, most fusion designs based on this assumption work badly without RGB or thermal images.

In this paper, instead of continuing previous works to find an optimal fusion feature for segmentation, we propose the *Variational Probabilistic Fusion Network (VPFNet)* for RGB-T semantic segmentation, which assumes that the optimal features for semantic segmentation are a series of fusion features within a certain range as shown in Fig.1 to alleviate the influence of modality noise, class-imbalance, and modality bias. Specifically, inspired by [15], [16], we regard fusion

Manuscript received August 19, 2023; revised August 16, 2023. The work is supported in part by Natural Science Foundation of Guangdong Province (China) under Grant 2022A1515010493, in part by the Fundamental Research Funds for the Central Universities (Sun Yat-sen University) under Grant 2021qntd11, in part by the Science Technology and Innovation Commission of Shenzhen Municipality under Grant 2021A03, in part by the Guangdong Basic and Applied Basic Research Foundation (2022B1515020103).

B. Lin, J. Zou and S. Fan are with the Institute for Advanced Study, University of Electronic Science and Technology of China, Shenzhen, 518107, China. Z. Lin, Y. Guo and Y. Zhang are with the School of Electronics and Communication Engineering, the Shenzhen Campus, Sun Yat-sen University, Shenzhen, 518107, China.

*B. Lin is the first author and corresponding author. {E-mail: linbaihong111@126.com}. Z. Lin is the co-first author.

features as random variables and propose a novel fusion module, i.e., *Variational Feature Fusion Module* (VFFM), to generate random samples of fusion features for segmentation. To avoid class-imbalance and modality bias, we employ the weighted cross-entropy loss and introduce Gaussian Mixture distribution as the prior of category and illumination for the proposed VFFM under variation framework. Using the above modeling, the final segmentation mask is predicted by averaging all segmentation confidence maps calculated from different random samples of fusion features to reduce sensitivity to modality noise. In brief, the contributions of this paper are listed as follows:

- VPFNet is proposed to obtain robust segmentation by regarding fusion features as random variables and averaging segmentation results under multiple samples of fusion features, which can alleviate the influence of modality noise, class-imbalance, and modality bias.
- VFFM is designed based on variation attention, and is controlled by category and illumination priors to generate random samples of fusion feature for multiple segmentation results. To our knowledge, it is the first work to break the unique fusion assumption.
- Experiments on MFNet and PST900 datasets demonstrate that the proposed fusion network achieves excellent segmentation performance compared with other state-of-the-art methods.

II. RELATED WORK

A. RGB-based Semantic Segmentation

Traditional RGB-based semantic segmentation methods utilized random forest [17] and conditional random field [18] to construct pixel-level classifiers to realize semantic segmentation based on hand-crafted features, such as histograms of oriented gradients [19] and scale-invariant feature transform [20].

Recently, deep learning methods have become the dominant solutions for RGB-based semantic segmentation since these methods can easily achieve remarkable results based on machine learnt features. Long *et al.* [21] first propose an efficient end-to-end Fully Convolutional Network for semantic segmentation to replace traditional semantic segmentation methods. However, Fully Convolutional Network cannot fully utilize boundary information laid in low level features. Thus, Ronneberger *et al.* [22] propose UNet for segmentation which can concatenate feature maps of different scales based on skip connections between encoder and decoder. To further enhance segmentation performance for objects of varying sizes, the Pooling Module [23] and the Atrous Spatial Pyramid Pooling [24] are introduced, which can extract multi-scale information from a feature map. Later, Attention-based models [25], [26] are designed, which can incorporate global semantic information into a feature map. The above-mentioned methods enhance the performance of RGB-based deep learning semantic segmentation from different aspects.

B. RGB-T Semantic Segmentation

Similarly, deep learning methods are widely adopted for RGB-T semantic segmentation. However, different from RGB-

based Semantic Segmentation, how to fuse deep complementary features from RGB and thermal images effectively is a key problem for RGB-T semantic segmentation.

Early methods employ addition [27], [28] or concatenation [5], [29] operations to directly fuse deep features of RGB and thermal images generated by feature extraction networks. To obtain better segmentation performance, these methods focus on different level features generation for fusion in network architecture. For instance, MFNet [5] generates different level features using two separate symmetric encoders for RGB and thermal images respectively and fuse them in a shared decoder. RTFNet [27] adopts heavyweight backbone ResNet-152s [30] to extract modality features, and fuses different level thermal features with RGB features in encoder stage. FuseSeg [28] employs DenseNet-161s [31] as backbone, and fuses the modality features in both encoder and decoder stages. PSTNet [29] introduces a dual-stream CNN to first extract the RGB semantic information, and then concatenate it to the thermal image to predict the final dense map. The above fusion strategies have been roughly divided into three categories [32], including decoder fusion [5], encoder fusion [8], [11], [27], [28], [33] and feature fusion [6], [10], [34]. However, recent studies point out that early fusion strategies based on addition or concatenation can easily introduce modality noise while incorporating complementary information [14]. What's more, these methods are facing bottlenecks and cannot achieve significantly-higher segmentation performance.

To overcome the bottlenecks caused by fusion strategies based on addition or concatenation, two kinds of solutions are proposed, including designing specific attention-mechanisms-based feature fusion modules [7]–[9], and introducing prior knowledge to supervise fusion models [6], [10], [11]. For the first kind of solutions, FEANet [8] employs FEAM, which sequentially uses channel and spatial attentions to extract complementary information and suppress modality noise from each single modality before fusing the features. ABMDRNet [7] introduces a MSC module and a MCC module to integrate cross-modal multiscale contextual information and their long-range dependencies along the spatial and channel dimensions respectively. DooDleNet [9] adopts a spatial attention module based on two rough confidence maps generated by RGB and thermal images respectively to deal with feature disagreement. For the second kind of solutions, GMNet [10] introduces boundary label, binary label, and class label to regularize different level fusion features of single modality. Similarly, MFFNet [11] introduces the same labels information to regularize fusion features. EGFNet [6] employs edge information to guide fusion features generation. The above fusion strategies achieve better segmentation performance compared with early fusion strategies. However, they try to find an optimal fusion feature for the best segmentation, leading to sensitivity to modality noise, class-imbalance, and modality bias.

III. PROPOSED METHOD

In this section, we first provide the overall architecture of VPFNet in Sec.III-A, then, introduce the core module of VPFNet, i.e., the *Variational Feature Fusion Module* (VFFM) in Sec.III-B. Finally, we provide the loss function in Sec.III-C.

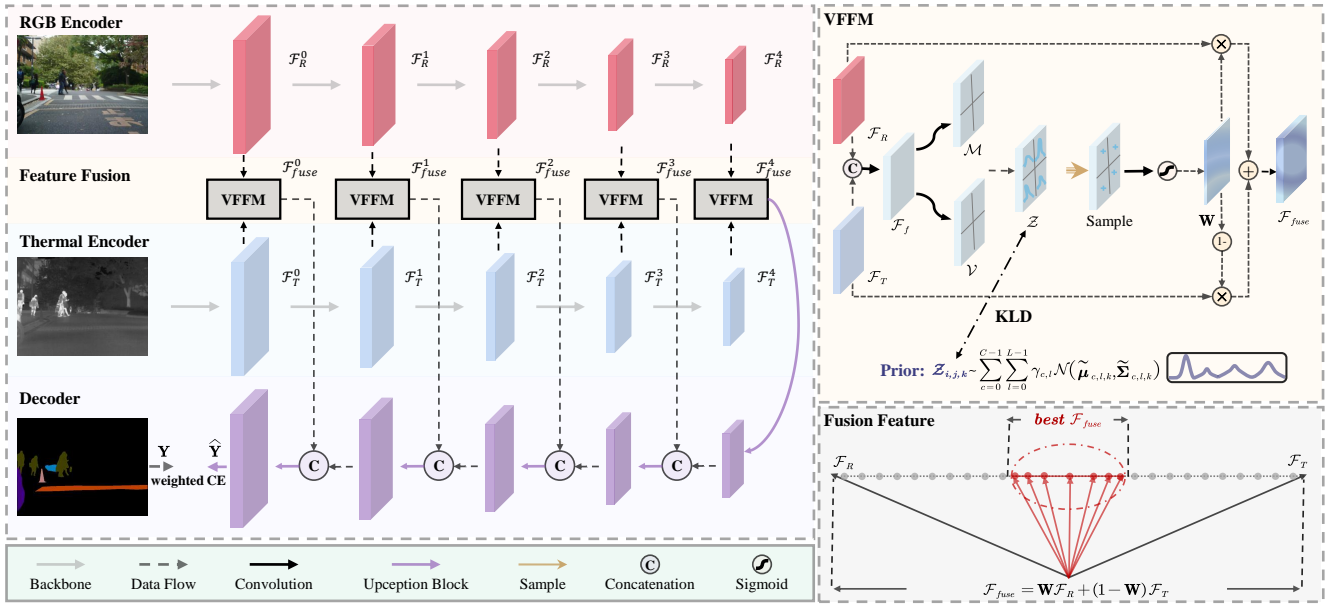


Fig. 2. Overall architecture of the proposed VPFNet.

A. Overall Architecture

The overall architecture of the proposed VPFNet for RGB-T semantic segmentation is shown in Fig.2, which consists of three parts, including the encoder part, the feature fusion part, and the decoder part. For the encoder part, we adopt two separate symmetric ResNet-50s [30] as backbones to extract the multi-level discriminative features from RGB and thermal images respectively. The pooling and the fully connected layer of ResNet-50s are removed to preserve spatial resolution. Then, we denote the extracted multi-level features of RGB and thermal images as $\{\mathcal{F}_R^i \mid i = 0, 1, 2, 3, 4\}$ and $\{\mathcal{F}_T^i \mid i = 0, 1, 2, 3, 4\}$ respectively. For the feature fusion part, in order to improve representation and generalization abilities, we propose a novel fusion module, VFFM, which regards fusion features as random variables. Using multiple VFFMs, we fuse multi-level features to obtain random samples of multi-level fusion features $\{\mathcal{F}_{fuse}^i \mid i = 0, 1, 2, 3, 4\}$. More details about VFFM will be introduced in Sec.III-B. For the decoder part, we combine multi-level fusion features generated by the feature fusion part to obtain the segmentation result using skip connections and Upception blocks proposed by [27]. Owing to high computational overhead, we remove two sequential 1×1 convolutions from the Upception blocks. As fusion features are random variables, we can obtain N_s segmentation results under N_s samples of fusion features, and obtain the final segmentation result \bar{Y} by averaging all confidence maps of N_s segmentation results to reduce sensitivity to modality noise.

B. Variational Feature Fusion Module

To improve generalization and representation abilities, we assume that the optimal features for semantic segmentation are a series of fusion features within a certain range. This assumption is reasonable: First, it can alleviate the sensitivity

of fusion features to class-imbalance, modality bias, and modality noise, since the decoder part is required to turn different samples of fusion features to the best segmentation under this assumption. Second, the fusion module based on this assumption can support different biased fusion features, since different RGB-biased and thermal-biased fusion features can be regarded as samples drawn from the fusion feature distribution as shown in Fig.1.

Based on the above assumption, we regard fusion features as random variables. Then, we propose a novel feature fusion module, the *Variational Feature Fusion Module* (VFFM), to fuse different modality features and generate random samples of a fusion feature, as shown in Fig.2. In VFFM, the fusion feature is represented as:

$$[\mathcal{F}_{fuse}]_{i,j,k} = \mathbf{W}_{i,j} [\mathcal{F}_R]_{i,j,k} + (1 - \mathbf{W}_{i,j}) [\mathcal{F}_T]_{i,j,k} \quad (1)$$

where \mathbf{W} is a spatial attention map and $\mathbf{W}_{i,j}$ denotes the attention value at the spatial coordinate (i, j) satisfying $0 \leq \mathbf{W}_{i,j} \leq 1$. When $\mathbf{W}_{i,j} = 1$, \mathcal{F}_{fuse} denotes RGB feature; when $\mathbf{W}_{i,j} = 0$, \mathcal{F}_{fuse} denotes thermal feature, as shown at bottom right corner of Fig.2. We also name $\mathbf{W}_{i,j}$ as a *fusion factor*, since it can affect the bias of feature fusion. To obtain different fusion results of \mathcal{F}_{fuse} , we regard $\mathbf{W}_{i,j}$ as a random variable. Then, the key problem of VFFM is how to design a neural network to obtain the random samples of $\mathbf{W}_{i,j}$.

Inspired by VAE [15] and DKPNet [16], we introduce a latent random 3D-tensor variable \mathcal{Z} to generate the samples of \mathbf{W} instead of directly modeling the distribution function of \mathbf{W} . Elements of \mathcal{Z} are assumed to be independently drawn from isotropic Gaussian distributions. Then, we design a network to calculate the means and variances of Gaussian distributions of \mathcal{Z} , and generate \mathbf{W} based on random samples of \mathcal{Z} . The network design is shown at the top right corner of Fig.2.

In VFFM, we first calculate the complementary intermediate fusion feature \mathcal{F}_f as the following:

$$\mathcal{F}_f = \sigma_L (\text{BN} (\text{Conv}_s (\text{Cat} (\mathcal{F}_R, \mathcal{F}_T); R/r))) \quad (2)$$

where Cat denotes concatenation, R denotes the number of channels of $\text{Cat} (\mathcal{F}_R, \mathcal{F}_T)$, r denotes the squeeze ratio, $\text{Conv}_s (*; R/r)$ denotes convolution with kernel size s and R/r output channels, BN denotes Batchnorm, and σ_L denotes LeakyReLU activate function with rate 0.2, which can enhance the feature representation ability [5]. Then, we use \mathcal{F}_f to generate the mean $\mathcal{M}_{i,j,k}$ and variance $\mathcal{V}_{i,j,k}$ of isotropic Gaussian distribution of $\mathcal{Z}_{i,j,k}$, i.e.,

$$\mathcal{Z}_{i,j,k} \sim \mathcal{N} (\mathcal{M}_{i,j,k}, \mathcal{V}_{i,j,k}) \quad (3a)$$

$$\mathcal{M} = \text{Conv}_1 (\mathcal{F}_f; d), \quad \log \mathcal{V} = \text{Conv}_1 (\mathcal{F}_f; d) \quad (3b)$$

where $\text{Conv}_1 (*; d)$ denotes a 1×1 convolutional block with d output channels. Finally, \mathbf{W} can be obtained by:

$$\mathbf{W} = \sigma_S (\text{Conv}_1 (\mathcal{Z}; 1)) \quad (4)$$

where $\text{Conv}_1 (*; 1)$ denotes 1×1 convolution with only one output channel, elements of \mathcal{Z} are drawn from the distribution of Eqn.(3). σ_S denotes Sigmoid activation function to normalize elements of \mathbf{W} between 0 and 1. Based on the above network and Eqn.(1), we can obtain the fusion feature sample of \mathcal{F}_{fuse} .

C. Loss Function

Theoretically, we can directly employ the cross-entropy loss as the RGB-T semantic segmentation loss. Using this loss function, the fusion network will be trained to obtain the best segmentation under different fusion feature samples of \mathcal{F}_{fuse} obtained from a pair of RGB and thermal images, thus, it is robust to modality noise. However, the cross-entropy loss does not take data class-imbalance [12] into consideration. Moreover, recent studies point out that uniform objective designed for all modalities could lead to under-optimized unimodal representations [13], i.e., modality bias.

To avoid class-imbalance and modality bias, we employ the weighted cross-entropy loss and introduce prior information (e.g., illumination and category) to control the fusion factor distribution $p(\mathbf{W})$. Specifically, inspired by DKPNet [16], we maximize the log-likelihood of the conditional probability $p(\mathbf{W} | \mathcal{F}_R, \mathcal{F}_T, \mathbf{Y}, l)$ as follows:

$$\begin{aligned} & \log (p(\mathbf{W} | \mathcal{F}_R, \mathcal{F}_T, \mathbf{Y}, l)) \\ &= \log \int q(\mathcal{Z} | \mathcal{F}_R, \mathcal{F}_T, \mathbf{Y}, l) \frac{p(\mathbf{W}, \mathcal{Z} | \mathcal{F}_R, \mathcal{F}_T, \mathbf{Y}, l)}{q(\mathcal{Z} | \mathcal{F}_R, \mathcal{F}_T, \mathbf{Y}, l)} dz \\ &\geq \mathbb{E}_{q(\mathcal{Z} | \mathcal{F}_R, \mathcal{F}_T, \mathbf{Y}, l)} [\log (p(\mathbf{W} | \mathcal{F}_R, \mathcal{F}_T, \mathbf{Y}, \mathcal{Z}, l))] \\ &\quad - KL [q(\mathcal{Z} | \mathcal{F}_R, \mathcal{F}_T, \mathbf{Y}, l) \| p(\mathcal{Z} | \mathcal{F}_R, \mathcal{F}_T, \mathbf{Y}, l)] \end{aligned} \quad (5)$$

where l denotes illumination scenario prior (e.g., day and night) of the input images, \mathbf{Y} denotes segmentation containing category prior of every pixel, $q(\mathcal{Z} | \mathcal{F}_R, \mathcal{F}_T, \mathbf{Y}, l)$ denotes the variational posterior distribution of Eqn.(3), $p(\mathcal{Z} | \mathcal{F}_R, \mathcal{F}_T, \mathbf{Y}, l)$ denotes the prior distribution of \mathcal{Z} .

According to [15], we can maximize the evidence lower bound (ELBO) as a proxy for maximizing the log-likelihood.

In Eqn(5), ELBO includes two terms. The first term $\mathbb{E}_q [\log (p(\mathbf{W} | \mathcal{F}_R, \mathcal{F}_T, \mathbf{Y}, \mathcal{Z}, l))]$ aims to generate the best fusion factor matrix \mathbf{W} from latent variables \mathcal{Z} to improve segmentation performance, i.e., it corresponds to segmentation estimation loss. Considering data class-imbalance [12], we describe this term as the weighted cross-entropy loss between the ground-truth segmentation \mathbf{Y} and the estimated segmentation $\hat{\mathbf{Y}}(\mathbf{W})$ based on the fusion factor matrix \mathbf{W} . The second term is the KL distance between the posterior distribution $q(\mathcal{Z} | \mathcal{F}_R, \mathcal{F}_T, \mathbf{Y}, l)$ and the prior distribution $p(\mathcal{Z} | \mathcal{F}_R, \mathcal{F}_T, \mathbf{Y}, l)$. This term can indirectly control the posterior distribution of fusion factor distribution $p(\mathbf{W})$ to alleviate modality bias [16] based on illumination and category prior information, since \mathbf{W} is obtained from \mathcal{Z} based on Eqn.(4).

To design the prior distribution $p(\mathcal{Z} | \mathcal{F}_R, \mathcal{F}_T, \mathbf{Y}, l)$, we assume that each element of \mathcal{Z} is independently drawn from Gaussian mixture distribution with $L \times C$ Gaussian components, and

$$\begin{aligned} & p(\mathcal{Z}_{i,j,k} | \mathcal{F}_R, \mathcal{F}_T, \mathbf{Y}_{i,j} = c, l) \\ & \approx p(\mathcal{Z}_{i,j,k} | \mathbf{Y}_{i,j} = c, l) = \mathcal{N} (\tilde{\boldsymbol{\mu}}_{c,l,k}, \tilde{\boldsymbol{\Sigma}}_{c,l,k}) \end{aligned} \quad (6a)$$

$$p(\mathbf{Y}_{i,j} = c, l) = \gamma_{c,l} \geq 0, \quad \sum_{c=0}^{C-1} \sum_{l=0}^{L-1} \gamma_{c,l} = 1 \quad (6b)$$

$$p(\mathcal{Z}_{i,j,k}) \approx \sum_{c=0}^{C-1} \sum_{l=0}^{L-1} \gamma_{c,l} \mathcal{N} (\tilde{\boldsymbol{\mu}}_{c,l,k}, \tilde{\boldsymbol{\Sigma}}_{c,l,k}), \quad (6c)$$

where C denotes the number of categories, L denotes the number of illumination conditions, $\tilde{\boldsymbol{\mu}}_{c,l,k}$ and $\tilde{\boldsymbol{\Sigma}}_{c,l,k}$ represent the mean and variance with different category and illumination condition respectively. In this paper, we only consider two illumination conditions, i.e., day and night, thus, $L = 2$. For convenience, we set $\gamma_{c,l} = \frac{1}{LC}$. As for $\tilde{\boldsymbol{\mu}}_{c,l,k}$ and $\tilde{\boldsymbol{\Sigma}}_{c,l,k}$, these parameters are set to be learnable during the training process, thus, prior of \mathcal{Z} can record the global statistical information of the training dataset.

Then, the KL distance in Eqn.(5) can be formulated as:

$$\begin{aligned} & KL [q(\mathcal{Z} | \mathcal{F}_R, \mathcal{F}_T, \mathbf{Y}, l) \| p(\mathcal{Z} | \mathcal{F}_R, \mathcal{F}_T, \mathbf{Y}, l)] \\ &= \frac{1}{D} \sum_{i,j,k} \frac{1}{2} \left[\log \frac{\tilde{\boldsymbol{\Sigma}}_{c,l,k}}{\mathcal{V}_{i,j,k}} + \text{tr} \left(\tilde{\boldsymbol{\Sigma}}_{c,l,k}^{-1} \mathcal{V}_{i,j,k} \right) - d \right. \\ & \quad \left. + (\tilde{\boldsymbol{\mu}}_{c,l,k} - \mathcal{M}_{i,j,k}) \tilde{\boldsymbol{\Sigma}}_{c,l,k}^{-1} (\tilde{\boldsymbol{\mu}}_{c,l,k} - \mathcal{M}_{i,j,k})^T \right] \end{aligned} \quad (7)$$

where d denotes the channel dimension of \mathcal{Z} , D denotes the number of elements in \mathcal{Z} , l denotes the illumination condition of each pair of RGB and thermal images, c denotes the pixel category label which is related to the segmentation mask of \mathcal{Z} at the spatial coordinate (i, j) . Since the spatial sizes of \mathcal{Z} and \mathbf{Y} are different, we resize the segmentation mask \mathbf{Y} using the nearest neighbor method to obtain the segmentation mask of \mathcal{Z} .

Based on the above modeling, the loss function of the proposed VPFNet can be formulated as:

$$L_{total} = \frac{1}{N_b} \sum_{b=1}^{N_b} \left(\text{WeightCE} (\hat{\mathbf{Y}}_b, \mathbf{Y}_b) + \beta \overline{KL}_b \right) \quad (8)$$

TABLE I
THE RESULTS OF VPFNET WITH DIFFERENT VALUES OF β .

β	0	0.3	0.5	0.7	1
mIoU	56.78	57.09	57.61	56.71	56.35

TABLE II
THE RESULTS OF PROBABILISTIC AND NON-PROBABILISTIC FUSION MODELS

Methods	non-prob. fusion without attention	non-prob. fusion with attention	probabilistic fusion (VPFNet without KL)
mAcc	69.96	68.70	71.08
mIoU	55.99	56.35	56.78

TABLE III
THE RESULTS OF VPFNET WITH DIFFERENT LOSS FUNCTIONS

Loss Func.	Car stop		Guardrail		mAcc	mIoU
	Acc	IoU	Acc	IoU		
CE	32.41	27.98	20.87	3.91	65.61	55.56
CE+KL	32.87	28.48	29.35	4.77	67.96	56.50
WeightCE	34.82	28.66	52.39	7.48	71.08	56.78
WeightCE + KL	38.33	31.67	46.32	9.40	70.91	57.61

TABLE IV
THE RESULTS OF VPFNET WITH DIFFERENT KL PRIOR REGULARIZATION

Loss Func.	Illumination	Category	mAcc	mIoU
without KL	-	-	71.08	56.78
KL with different prior information	✓		69.81	56.61
	✓	✓	69.51	56.88
			70.91	57.61

TABLE V
THE RESULTS OF VPFNET UNDER DIFFERENT VALUES OF N_s

N_s	1*	5	10	20	50
mAcc	70.91	69.75	69.72	69.77	69.82
mIoU	57.61	57.62	57.65	57.71	57.72

* $N_s = 1$ means directly adopting the mean of latent variable \mathcal{Z} to generate fusion feature.

where $\text{WeightCE}(*, *)$ denotes the weighted cross-entropy loss between ground-truth label \mathbf{Y} and segmentation prediction $\hat{\mathbf{Y}}$ following [35], \overline{KL} denotes the average KL distance of Eqn.(7) for all VFFMs used to generate multi-level features, N_b denotes the number of RGB-thermal image pairs in the training mini-batch. β is a hyper-parameter to avoid posterior collapse following [36].

IV. EXPERIMENTS

A. Experiment Setup

1) *Datasets*: We conduct experiments on MFNet [5] dataset and PST900 [29] dataset, which are the only two public datasets for RGB-T semantic segmentation. For MFNet dataset, it contains 1569 pairs of annotated RGB and thermal images with 8 object categories in addition to the background category, including 820 pairs of images captured at daytime and 749 pairs of images captured at nighttime. Both RGB and thermal images have the same spatial resolution of 480×640 . For fairness, we directly adopt the dataset splitting scheme following [5]. For PST900 dataset, it consists of 894 pairs

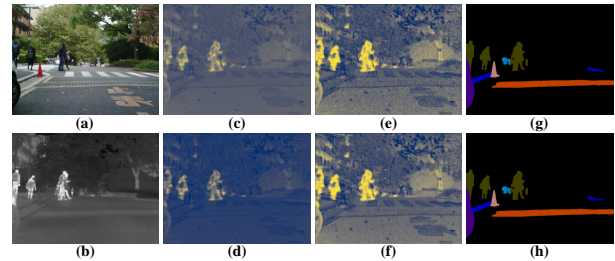


Fig. 3. Visualization example for the probabilistic fusion model. (a)-(h) RGB image, thermal image, the mean of latent variable \mathcal{Z} , the variance of latent variable \mathcal{Z} , a random sample of fusion feature, the average of five fusion feature samples, the segmentation result under a fusion feature sample, the average segmentation result under five fusion feature samples.

aligned RGB and thermal images captured at nighttime with 4 object categories in addition to the background category. Following [6], we resize the resolution of image to 640×1280 . Then, we adopt the same training, testing and verification setting as in [29].

2) *Evaluation Metrics*: Mean accuracy (mAcc) and mean intersection over union (mIoU) are adopted to evaluate the performance of different semantic segmentation models following previous related works [5]–[7], [27].

3) *Implementation Details*: The proposed VPFNet is implemented by PyTorch 1.11.0, CUDA 11.3, and Python 3.9.13. For training, the backbone is pretrained on ImageNet [37]. Then, following the training strategy in [6], we use random flipping and random cropping for data augmentation, and train the proposed VPFNet to its convergence within 300 epochs using the Ranger optimizer [38] with an initial learning rate and weight decay of $5e-5$ and $5e-4$ respectively. The training mini-batch size N_b is set to 3 in Eqn.(8). We run all experiments on a NVIDIA-V100 GPU.

B. Ablation Study

In this section, we first discuss the selection of hyperparameters in VPFNet. Then, we validate the effectiveness of each modeling component in the proposed VPFNet, including probabilistic fusion, loss function, and KL prior regularization. All experiments in this section are conducted based on MFNet dataset.

1) *Selection of Hyperparameters*: We first select the value of hyperparameters s , r , and d in Eqn.(2) and Eqn.(3). We carried out ablation experiments with $s \in \{3, 5, 7\}$, $r \in \{8, 16, 32\}$ and $d \in \{2, 4, 6, 8, 10\}$, and found VPFNet works best when $s = 7$, $r = 16$ and $d = 8$.

Then, we select the value of weight factor β in Eqn.(8). Theoretically, if β is too big, the KL prior regularization term in Eqn.(8) will weaken feature representation ability; if β is too small, the regularization term will have little influence on segmentation performance. Thus, we carry out ablation experiments with $\beta \in \{0, 0.3, 0.5, 0.7, 1\}$. The results are shown in Table I. From Table I, we can find that VPFNet can achieve the best performance when $\beta = 0.5$.

Moreover, we select the value of N_s mentioned in Sec.???. Theoretically, the segmentation result tends to be stable with the increase of N_s . However, N_s is required to be small

TABLE VI

RESULTS ON THE MFNET DATASET. '-' DENOTES THAT THE CORRESPONDING RESULTS ARE MISSED IN [29]. FOR RGB-BASED METHODS, 3C MEANS THE INPUT IMAGES ARE RGB IMAGES AND 4C MEANS THE INPUT IMAGES ARE 4 CHANNELS RGB-T IMAGES. FOR RGB-D METHODS, WE REPLACE THE DEPTH IMAGES WITH THERMAL IMAGES.

Methods	Type	Year	Car		Person		Bike		Curve		Car Stop		Guardrail		Color Cone		Bump		mAcc	mIoU
			Acc	IoU	Acc	IoU	Acc	IoU	Acc	IoU	Acc	IoU	Acc	IoU	Acc	IoU	Acc	IoU		
CCNet-3c	RGB	ICCV 2019	87.92	80.28	56.56	45.82	74.33	58.13	34.30	26.78	32.96	25.19	26.64	4.49	41.92	36.08	46.19	36.22	55.52	45.56
CCNet-4c	RGB	ICCV 2019	88.07	81.97	61.09	51.88	74.35	59.53	46.83	36.27	28.06	22.71	2.84	0.55	43.37	37.07	51.14	44.19	54.98	47.95
DANet-3c	RGB	CVPR 2019	88.83	80.07	54.63	44.31	72.04	57.38	27.66	22.30	33.86	25.89	22.70	4.21	37.19	31.73	46.42	35.28	53.57	44.24
DANet-4c	RGB	CVPR 2019	85.73	80.48	58.69	49.63	70.22	57.14	45.11	35.38	27.42	22.57	29.80	5.93	36.08	32.34	46.74	38.01	55.43	46.53
FuseNet	RGBD	ACCV 2016	81.00	75.60	75.20	66.30	64.50	51.90	51.00	37.80	17.40	15.00	0.00	0.00	31.10	21.40	51.90	45.00	52.40	45.60
D-CNN	RGBD	ECCV 2018	85.20	77.00	61.70	53.40	76.00	56.50	40.20	30.90	41.30	29.30	22.80	8.50	32.90	30.10	36.50	32.30	55.10	46.10
SAGate	RGBD	ECCV2020	86.00	73.80	80.80	59.20	69.40	51.30	56.70	38.40	24.70	19.30	0.00	0.00	56.90	24.50	52.10	48.80	58.30	45.80
MFNet	RGBT	IROS 2017	77.20	65.90	67.00	58.90	53.90	42.90	36.20	29.90	12.50	9.90	0.10	0.00	30.30	25.20	30.00	27.70	45.10	39.70
RTFNet-50	RGBT	RA-L 2019	91.30	86.30	78.20	67.80	71.50	58.20	69.80	43.70	32.10	24.30	13.40	3.60	40.40	26.00	73.50	57.20	62.20	51.70
RTFNet-152	RGBT	RA-L 2019	93.00	87.40	79.30	70.30	76.80	62.70	60.70	45.30	38.50	29.80	0.00	0.00	45.50	29.10	74.70	55.70	63.10	53.20
PSTNet	RGBT	ICRA 2020	-	76.80	-	52.60	-	55.30	-	29.60	-	25.10	-	15.10	-	39.40	-	45.00	-	48.40
FuseSeg-161	RGBT	T-ASE 2021	93.10	87.90	81.40	71.70	78.50	64.60	68.40	44.80	29.10	22.70	63.70	6.40	55.80	46.90	66.40	47.90	70.60	54.50
FEANet	RGBT	IROS 2021	93.30	87.80	82.70	71.10	76.70	61.10	65.50	46.50	26.60	22.10	70.80	6.60	66.60	55.30	77.30	48.90	73.20	55.30
ABMDRNet	RGBT	CVPR 2021	94.30	84.80	90.00	69.60	75.70	60.30	64.00	45.10	44.10	33.10	31.00	5.10	61.70	47.40	66.20	50.00	69.50	54.80
EGFNet	RGBT	AAAI 2022	95.80	87.60	89.00	69.80	80.60	58.80	71.50	42.80	48.70	33.80	33.60	7.00	65.30	48.30	71.10	47.10	72.70	54.80
MDRNet+	RGBT	TNNLS 2023	95.20	87.10	92.50	69.80	76.20	60.90	72.00	47.80	42.30	34.20	66.80	8.20	64.80	50.20	63.50	55.00	74.70	56.80
Ours	RGBT	-	93.43	87.10	87.70	73.97	73.82	62.57	68.84	48.15	38.33	31.67	46.32	9.40	60.06	52.25	70.69	55.31	70.91	57.61

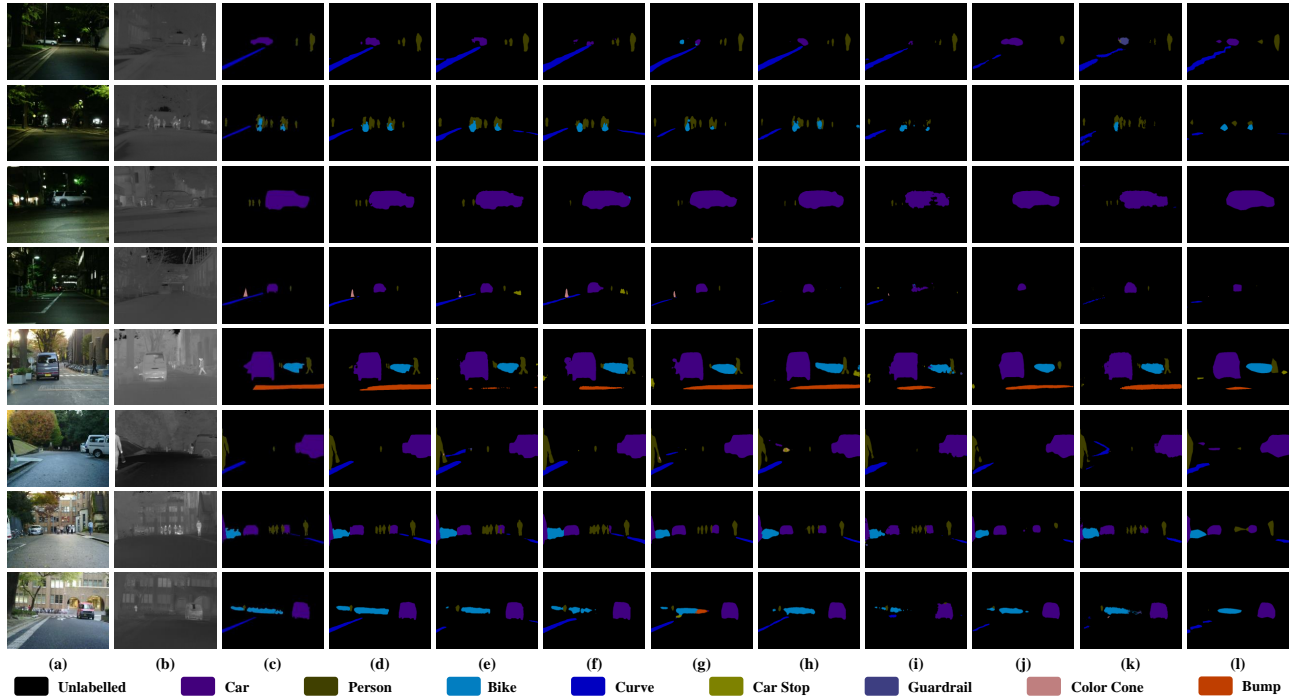


Fig. 4. Visual comparisons of different methods. (a) RGB images; (b) Thermal images; (c) Ground Truth; (d) Ours; (e) MDRNet; (f) EGFNet; (g) FEANet; (h) RTFNet; (i) MFNet; (j) SA-Gate; (k) FuseNet; (l) CCNet.

considering the balance of computational cost and performance. Thus, we carry out ablation experiments with $N_s \in \{1, 5, 10, 20, 50\}$. The results are shown in Table V. From the results, we can find that the mIoU value tends to be stable when $N_s \geq 20$. However, mIoU values at $N_s \geq 20$ are only slightly better than that at $N_s = 1$. Thus, for convenience, we approximate the average segmentation result by directly using the mean of \mathcal{Z} to generate the fusion feature sample.

2) *Effectiveness of Probabilistic Fusion*: To validate the effectiveness of probabilistic fusion, we design probabilistic and non-probabilistic fusion models based on VPFNet for comparison. The comparison results are shown in Table II. The non-probabilistic fusion model without attention is designed by replacing VFFM with element-wise addition to fuse modal-

ity features in VPFNet; The non-probabilistic fusion model with attention is designed by directly utilizing the mean \mathcal{M} to replace the random sample \mathcal{Z} in Eqn.(4) (i.e., deleting the variance \mathcal{V} and the random sampling process); The probabilistic fusion model is VPFNet without KL prior regularization. All these fusion models share the same weighted cross-entropy loss. From Table II, we can find that the probabilistic fusion model outperforms two non-probabilistic fusion models under different evaluation metrics, which prove the effectiveness of probabilistic fusion.

To further show the advantage of probabilistic fusion, we display a visualization example in Fig.3. From Fig.3, we can find that the fusion feature in Fig.3(e) is noisier than the average feature in Fig.3(f). However, the segmentation result

TABLE VII
RESULTS FROM DAYTIME AND NIGHTTIME IMAGES.

Methods	Type	Daytime		Nighttime	
		mAcc	mIoU	mAcc	mIoU
CCNet-3c	RGB	50.26	41.70	50.30	42.72
CCNet-4c	RGB	48.67	41.54	51.89	46.59
DANet-3c	RGB	50.18	41.05	48.20	41.45
DANet-4c	RGB	48.48	41.12	51.78	45.02
FuseNet	RGBD	46.71	40.13	49.11	42.02
D-CNN	RGBD	50.60	42.40	50.70	43.20
SA-Gate	RGBD	49.30	37.90	56.90	45.60
MFNet	RGBT	42.60	36.10	41.40	36.80
RTFNet-152	RGBT	60.00	45.80	60.70	54.80
FuseSeg-16l	RGBT	62.10	47.80	67.30	54.60
FEANet	RGBT	51.57	39.85	56.60	50.09
ABMDRNet	RGBT	58.40	46.70	68.30	55.50
EGFNet	RGBT	74.40	47.30	68.00	55.00
MDRNet+	RGBT	59.19	47.71	71.95	55.60
Ours	RGBT	63.29	50.32	67.81	56.64

TABLE VIII
RESULTS WHEN THE INPUT IMAGES LACK A CERTAIN MODAL INFORMATION. ONLY RGB AND ONLY THERMAL MEAN THE INPUT IMAGES ARE RGB IMAGES OR THERMAL IMAGES (WE SET THE MISSING MODALITY TO ZERO WHEN TESTING).

Methods	Type	Only RGB		Only Thermal		Worst Modality	
		mAcc	mIoU	mAcc	mIoU	mAcc	mIoU
FuseNet	RGBD	11.11	10.31	41.33	36.85	11.11	10.31
SAGate	RGBD	32.01	30.57	13.34	12.51	13.34	12.51
MFNet	RGBT	26.62	24.78	19.65	16.64	19.65	16.64
RTFNet	RGBT	44.89	37.30	26.41	24.57	26.41	24.57
FEANet	RGBT	15.96	8.69	58.35	48.72	15.96	8.69
MDRNet	RGBT	57.11	45.89	41.98	30.19	41.98	30.19
Ours	RGBT	48.14	41.08	42.20	35.80	42.20	35.80

of Fig.3(g) is nearly the same as that of Fig.3(h) despite that it is obtained based on noisy fusion feature, which prove that the segmentation based on probabilistic fusion is robust to noise.

3) *Effectiveness of Loss Function*: To validate the effectiveness of loss function, we design different loss functions for comparison, as shown in Table III. In Table III, we additionally provide the results of two categories, Car stop and Guardrail, which have only a few training samples. From the results, we can find that the weight cross entropy (WeightCE) loss can alleviate class-imbalance and enhance the segmentation performance compared with the cross entropy (CE) loss. Besides, the KL prior regularization in Eqn.(8) is necessary, since it can significantly enhance segmentation performance coordinated with the CE or WeightCE loss.

To further analyze the effectiveness of KL prior regularization, we design KL prior regularization with different prior information based on Eqn.(6) for comparison, as shown in Table IV. From the results, we can find that the segmentation performance under mIoU metric is significantly enhanced when considering both illumination and categories prior information. However, the segmentation performance is slightly worse when only considering prior of two illumination conditions (i.e., day and night.). The main reason is that the KL prior regularization of illumination is too coarse to introduce correct information for VFFM. The segmentation performance achieves about 0.1% improvement when only

considering category prior information, i.e., the number of Gaussian components is set to 9 in Eqn.(6). Obviously, KL prior regularization based on Gaussian mixture distribution in Eqn.(6) should have more Gaussian components, otherwise, it will not bring in significant improvement on segmentation performance. In the future work, we will try to further improve the modeling of KL prior regularization.

C. Comparison with State-of-the-Arts

1) *Comparison on MFNet Dataset*: We compare the proposed VPFNet with 13 state-of-the-art (SOTA) methods, including 2 deep learning RGB-based semantic segmentation methods (DANet [25], CCNet [26]), 3 RGB-D semantic segmentation methods (FuseNet [39], Depth-aware CNN [40], SAGate [14]), and 8 RGB-T semantic segmentation methods (MFNet [5], RTFNet [27], PSTNet [29], FuseSeg [28], FEANet [8], ABMDRNet [7], EGFNet [6], MDRNet+ [41]). The comparison results are shown in Table VI and Fig.4. From the results, we can find that although the proposed VPFNet does not show the best performance under most categories, it outperforms other state-of-the-art methods under mIoU metric when considering all categories, i.e., VPFNet has more balanced performance for different categories. Since the number of samples are not the same for different categories in the dataset, these results prove that VPFNet can simultaneously learn effective representations of all categories even if there exists class-imbalance [12] in the training data.

Moreover, we summarize the evaluation results from daytime and nighttime images respectively in Table VII. From the results, we can find that our proposed VPFNet still keep the state-of-the-art performance under mIoU metric. Additionally, the thermal images are more important at nighttime despite that it contains serious noise. However, compared with other methods, VPFNet performs far more better at nighttime, which proves that VPFNet is more robust to modality noise [13] of thermal images.

Besides, we discuss RGB-T semantic segmentation when losing an unknown modality. This scene occurs in realworld when one of RGB and thermal cameras is broken. To simulate this scene, we set the lost modality to zero and compare VPFNet with other methods, as shown in Table VIII. From the results, we can find that most segmentation methods based on the unique fusion feature assumption usually work badly without RGB images or thermal images, especially the FEANet [8]. Although the proposed VPFNet does not show the best performance under a certain modality, it outperforms other methods when considering the worst performance under unknown lost modality. Thus, VPFNet has more balanced performance for different modalities, which prove that VPFNet is more robust to modality bias [14] and has powerful representation ability.

2) *Comparison on PST900 Dataset*: We compare the proposed VPFNet with other state-of-the-art methods on the PST900 dataset [29]. Different from the MFNet dataset, all images in PST900 dataset are taken under poor light condition. Thus, we only introduce category prior information for the proposed VPFNet in training process. The comparison results

TABLE IX
RESULTS FROM PST900 DATASET [29].

Methods	Type	Background		Hand-Drill		Backpack		Fire-Extinguisher		Survivor		mAcc	mIoU
		Acc	IoU	Acc	IoU	Acc	IoU	Acc	IoU	Acc	IoU		
CCNet-4c	RGB	99.62	98.95	74.62	55.93	86.09	78.82	65.15	49.24	57.51	52.77	76.60	67.14
DANet-4c	RGB	99.74	99.02	82.80	68.28	83.28	78.49	58.16	48.05	54.73	50.46	75.74	68.86
ACNet	RGBD	99.83	99.25	53.59	51.46	85.56	83.19	84.88	59.95	69.10	65.19	78.67	71.81
SA-Gate	RGBD	99.74	99.25	89.88	81.01	89.03	79.77	80.70	72.97	64.19	62.22	84.71	79.05
MFNet	RGBT	98.89	97.85	68.59	4.87	77.49	63.02	57.15	37.31	15.40	8.63	63.50	50.34
RTFNet-50	RGBT	99.74	98.89	64.07	52.24	73.08	67.91	69.78	54.46	58.19	54.11	72.97	65.52
PSTNet	RGBT	-	98.85	-	53.60	-	69.20	-	70.12	-	50.03	-	68.36
ABMDRNet	RGBT	99.78	99.00	81.24	61.52	71.41	67.91	76.49	66.22	66.40	62.02	79.06	71.33
EGFNet	RGBT	99.48	99.26	97.99	64.67	94.17	83.05	95.17	71.29	83.30	74.30	94.02	78.51
MDRNet+	RGBT	99.30	99.07	90.17	63.04	93.53	76.27	86.63	63.47	85.56	71.26	91.04	74.62
Ours	RGBT	99.70	99.36	93.45	73.14	87.48	81.99	92.74	77.66	83.91	74.88	91.46	81.41

are summarized in Table IX. From the results, we can find that VPFNet outperforms other methods under mIoU metric when considering all categories. Besides, VPFNet has more balanced performance for different categories compared with other methods. These results are similar to that on the MFNet dataset, which prove high generalization ability of VPFNet.

V. CONCLUSION

In this paper, we propose a novel VPFNet for RGB-T semantic segmentation. The proposed network regards fusion features as random variables, generates random samples of fusion feature via a novel VFFM based on variation attention, and obtains the robust segmentation by averaging all segmentation results of different fusion feature samples. Experiments on two public datasets prove that the proposed VPFNet has the state-of-the-art segmentation performance. Moreover, extensive experimental results show that VPFNet has more balanced segmentation performance for different categories and modalities, and it is more robust to class-imbalance, modality noise, and modality bias.

REFERENCES

- [1] F. Nesti, G. Rossolini, S. Nair, A. Biondi, and G. Buttazzo, "Evaluating the robustness of semantic segmentation for autonomous driving against real-world adversarial patch attacks," in *proc. IEEE Winter Conf. on Applications of Comput. Vis.*, 2022, pp. 2280–2289.
- [2] H. Wang, Y. Chen, Y. Cai, L. Chen, Y. Li, M. A. Sotelo, and Z. Li, "Sfnet-n: An improved sfnet algorithm for semantic segmentation of low-light autonomous driving road scenes," *IEEE Trans. Intell. Transp. Syst.*, vol. 23, no. 11, pp. 21405–21417, 2022.
- [3] I. Alonso, L. Riazuelo, and A. C. Murillo, "Mininet: An efficient semantic segmentation convnet for real-time robotic applications," *IEEE Trans. Robotics*, vol. 36, no. 4, pp. 1340–1347, 2020.
- [4] S. Ainetter and F. Fraundorfer, "End-to-end trainable deep neural network for robotic grasp detection and semantic segmentation from rgb," in *IEEE Int. Conf. on Robotics and Automation (ICRA)*. IEEE, 2021, pp. 13452–13458.
- [5] Q. Ha, K. Watanabe, T. Karasawa, Y. Ushiku, and T. Harada, "Mfnet: Towards real-time semantic segmentation for autonomous vehicles with multi-spectral scenes," in *IEEE Int. Conf. on Intell. Robots and Systems (IROS)*. IEEE, 2017, pp. 5108–5115.
- [6] W. Zhou, S. Dong, C. Xu, and Y. Qian, "Edge-aware guidance fusion network for rgb-thermal scene parsing," in *proc. AAAI Conf. Artif. Intell.*, 2022, pp. 3571–3579.
- [7] Q. Zhang, S. Zhao, Y. Luo, D. Zhang, N. Huang, and J. Han, "Abmdrnet: Adaptive-weighted bi-directional modality difference reduction network for rgb-t semantic segmentation," in *proc. IEEE Conf. Comput. Vis. Pattern Recognit. (CVPR)*, 2021, pp. 2633–2642.
- [8] F. Deng, H. Feng, M. Liang, H. Wang, Y. Yang, Y. Gao, J. Chen, J. Hu, X. Guo, and T. L. Lam, "Feanet: Feature-enhanced attention network for rgb-thermal real-time semantic segmentation," in *IEEE Int. Conf. on Intell. Robots and Systems (IROS)*. IEEE, 2021, pp. 4467–4473.
- [9] O. Frigo, L. Martin-Gaffe, and C. Wacongne, "Doodlenet: Double deeplab enhanced feature fusion for thermal-color semantic segmentation," in *proc. IEEE Conf. Comput. Vis. Pattern Recognit. (CVPR)*, 2022, pp. 3021–3029.
- [10] W. Zhou, J. Liu, J. Lei, L. Yu, and J.-N. Hwang, "Gmnet: graded-feature multilabel-learning network for rgb-thermal urban scene semantic segmentation," *IEEE Trans. Image Processing*, vol. 30, pp. 7790–7802, 2021.
- [11] W. Zhou, X. Lin, J. Lei, L. Yu, and J.-N. Hwang, "Mffenet: Multiscale feature fusion and enhancement network for rgb-thermal urban road scene parsing," *IEEE Trans. Multimedia*, vol. 24, pp. 2526–2538, 2021.
- [12] T. Zhou, S. Ruan, and S. Canu, "A review: Deep learning for medical image segmentation using multi-modality fusion," *Array*, vol. 3, p. 100004, 2019.
- [13] X. Peng, Y. Wei, A. Deng, D. Wang, and D. Hu, "Balanced multimodal learning via on-the-fly gradient modulation," in *proc. IEEE Conf. Comput. Vis. Pattern Recognit. (CVPR)*, 2022, pp. 8238–8247.
- [14] X. Chen, K.-Y. Lin, J. Wang, W. Wu, C. Qian, H. Li, and G. Zeng, "Bi-directional cross-modality feature propagation with separation-and-aggregation gate for rgb-d semantic segmentation," in *proc. Eur. Conf. Comput. Vis. (ECCV)*. Springer, 2020, pp. 561–577.
- [15] D. P. Kingma and M. Welling, "Auto-encoding variational bayes," *arXiv preprint arXiv:1312.6114*, 2013.
- [16] B. Chen, Z. Yan, K. Li, P. Li, B. Wang, W. Zuo, and L. Zhang, "Variational attention: Propagating domain-specific knowledge for multi-domain learning in crowd counting," in *proc. IEEE Int. Conf. Comput. Vis. (ICCV)*, 2021, pp. 16065–16075.
- [17] L. Breiman, "Random forests," *Machine learning*, vol. 45, pp. 5–32, 2001.
- [18] J. Lafferty, A. McCallum, and F. C. Pereira, "Conditional random fields: Probabilistic models for segmenting and labeling sequence data," in *proc. IEEE int. conf. on Machine Learning (ICML)*, 2001, pp. 282–289.
- [19] N. Dalal and B. Triggs, "Histograms of oriented gradients for human detection," in *proc. IEEE Conf. Comput. Vis. Pattern Recognit. (CVPR)*, vol. 1. Ieee, 2005, pp. 886–893.
- [20] W. Burger and M. J. Burge, *Scale-Invariant Feature Transform (SIFT)*. London: Springer London, 2016, pp. 609–664. [Online]. Available: https://doi.org/10.1007/978-1-4471-6684-9_25
- [21] J. Long, E. Shelhamer, and T. Darrell, "Fully convolutional networks for semantic segmentation," in *proc. IEEE Conf. Comput. Vis. Pattern Recognit. (CVPR)*, 2015, pp. 3431–3440.
- [22] O. Ronneberger, P. Fischer, and T. Brox, "U-net: Convolutional networks for biomedical image segmentation," in *proc. Int. Conf. Medical Image Computing and Computer-Assisted Intervention (MICCAI)*. Springer, 2015, pp. 234–241.
- [23] H. Zhao, J. Shi, X. Qi, X. Wang, and J. Jia, "Pyramid scene parsing network," in *proc. IEEE Conf. Comput. Vis. Pattern Recognit. (CVPR)*, 2017, pp. 2881–2890.
- [24] L.-C. Chen, G. Papandreou, I. Kokkinos, K. Murphy, and A. L. Yuille, "Deeplab: Semantic image segmentation with deep convolutional nets, atrous convolution, and fully connected crfs," *IEEE Trans. Pattern Anal. Machine Intell.*, vol. 40, no. 4, pp. 834–848, 2017.

- [25] J. Fu, J. Liu, H. Tian, Y. Li, Y. Bao, Z. Fang, and H. Lu, "Dual attention network for scene segmentation," in *proc. IEEE Conf. Comput. Vis. Pattern Recognit. (CVPR)*, 2019, pp. 3146–3154.
- [26] Z. Huang, X. Wang, L. Huang, C. Huang, Y. Wei, and W. Liu, "Cnet: Criss-cross attention for semantic segmentation," in *proc. IEEE Int. Conf. Comput. Vis. (ICCV)*, 2019, pp. 603–612.
- [27] Y. Sun, W. Zuo, and M. Liu, "Rtfnnet: Rgb-thermal fusion network for semantic segmentation of urban scenes," *IEEE Robotics and Automation Letters*, vol. 4, no. 3, pp. 2576–2583, 2019.
- [28] Y. Sun, W. Zuo, P. Yun, H. Wang, and M. Liu, "Fuseseg: Semantic segmentation of urban scenes based on rgb and thermal data fusion," *IEEE Trans. Automation Science and Engineering*, vol. 18, no. 3, pp. 1000–1011, 2020.
- [29] S. S. Shivakumar, N. Rodrigues, A. Zhou, I. D. Miller, V. Kumar, and C. J. Taylor, "Pst900: Rgb-thermal calibration, dataset and segmentation network," in *proc. IEEE int. conf. on robotics and automation (ICRA)*. IEEE, 2020, pp. 9441–9447.
- [30] K. He, X. Zhang, S. Ren, and J. Sun, "Deep residual learning for image recognition," in *proc. IEEE Conf. Comput. Vis. Pattern Recognit. (CVPR)*, 2016, pp. 770–778.
- [31] G. Huang, Z. Liu, L. Van Der Maaten, and K. Q. Weinberger, "Densely connected convolutional networks," in *proc. IEEE Conf. Comput. Vis. Pattern Recognit. (CVPR)*, 2017, pp. 4700–4708.
- [32] G. Li, Y. Wang, Z. Liu, X. Zhang, and D. Zeng, "Rgb-t semantic segmentation with location, activation, and sharpening," *IEEE Trans. Circuits and Syst. Video Technol.*, 2022.
- [33] Z. Guo, X. Li, Q. Xu, and Z. Sun, "Robust semantic segmentation based on rgb-thermal in variable lighting scenes," *Measurement*, vol. 186, p. 110176, 2021.
- [34] J. Liu, W. Zhou, Y. Cui, L. Yu, and T. Luo, "Gcnet: Grid-like context-aware network for rgb-thermal semantic segmentation," *Neurocomputing*, vol. 506, pp. 60–67, 2022.
- [35] A. Paszke, A. Chaurasia, S. Kim, and E. Culurciello, "Enet: A deep neural network architecture for real-time semantic segmentation," *arXiv preprint arXiv:1606.02147*, 2016.
- [36] I. Higgins, L. Matthey, A. Pal, C. Burgess, X. Glorot, M. Botvinick, S. Mohamed, and A. Lerchner, "beta-vae: Learning basic visual concepts with a constrained variational framework," in *proc. Int. conf. on learning representations (ICLR)*, 2017.
- [37] J. Deng, W. Dong, R. Socher, L.-J. Li, K. Li, and L. Fei-Fei, "Imagenet: A large-scale hierarchical image database," in *proc. IEEE Conf. Comput. Vis. Pattern Recognit. (CVPR)*. Ieee, 2009, pp. 248–255.
- [38] L. Wright and N. Demeure, "Ranger21: a synergistic deep learning optimizer," *arXiv preprint arXiv:2106.13731*, 2021.
- [39] C. Hazirbas, L. Ma, C. Domokos, and D. Cremers, "Fusenet: Incorporating depth into semantic segmentation via fusion-based cnn architecture," in *proc. Asian Conf. on Comput. Vis. (ACCV)*. Springer, 2017, pp. 213–228.
- [40] W. Wang and U. Neumann, "Depth-aware cnn for rgb-d segmentation," in *proc. Eur. Conf. Comput. Vis. (ECCV)*, 2018, pp. 135–150.
- [41] S. Zhao, Y. Liu, Q. Jiao, Q. Zhang, and J. Han, "Mitigating modality discrepancies for rgb-t semantic segmentation," *IEEE Trans. Neural Networks Learn. Syst.*, 2023.